Pathological implications of APP clustering and its effect on β-Secretase cleavage

![IISER PUNE logo]

Master's Thesis

Author:

Pratyush Ramakrishna

BS-MS student
Roll no: 20131133
IISER, Pune

Supervisor:

Dr. Suhita Nadkarni
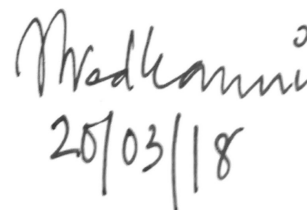
Assistant Professor
Department of Biology
IISER, Pune

Certificate

This is to certify that this dissertation entitled "Pathological implications of APP clustering and its effect on β-Secretase cleavage" towards the partial fulfilment of the BS-MS dual degree programme at the Indian Institute of Science Education and Research, Pune represents study/work carried out by Pratyush Ramakrishna at the Indian Institute of Science Education and Research, Pune under the supervision of Dr. Suhita Nadkarni, Assistant Professor, Department of Biology, during the academic year 2017-2018.
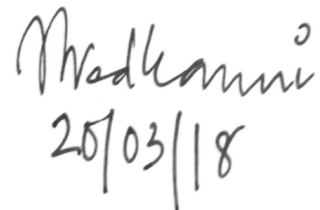
Pratyush Ramakrishna

Dr. Suhita Nadkarni

Declaration

I hereby declare that the matter embodied in the report entitled "Pathological implications of APP clustering and its effect on β-Secretase cleavage" are the results of the work carried out by me at the Department of Biology, Indian Institute of Science Education and Research, Pune, under the supervision of Dr. Suhita Nadkarni and the same has not been submitted elsewhere for any other degree.

`

20/03/18

Pratyush Ramakrishna   **Dr. Suhita Nadkarni**

Acknowledgements

Abstract

Alzheimers disease(AD) is one of the most prevalent and debilitating neurodegenerative diseases. One of the indicators of AD pathology is the presence of Amyloid Beta(Aβ) plaques in different regions of the brain. Aβ molecules aggregate to form plaques due to the excess production or improper clearance of Aβ. It is therefore of paramount importance to study the reactions involved in the production of Aβ. Aβ is formed when Amyloid Precursor Protein (APP), a transmembrane protein found abundantly in neurons is sequentially cleaved by β- and γ-Secretase.This project focuses on the interactions between APP and β-Secretase. From experimental data, we know that APP forms clusters on the synaptic membrane.Motivated by experimental observations of clustering and localization of APP, we use a Monte-Carlo based spatially realistic model to recreate these APP interactions.We also systematically reproduce a range of aberrant biophysical properties observed in AD, quantify its consequences and discuss its effects on APP cleavage. Our calculations inferred that differential APP clustering and affinities to β-Secretase can modulate the Aβ produced.As APP cleavage is the penultimate step in the production of Aβ, understanding the details of its synaptic localization and its processing can provide valuable insights into Aβ pathology.

Contents

List of Figures

List of Tables

1 Introduction

Alzheimers Disease (AD) is one of the most prevalent neurodegenerative diseases. Short term memory loss, coupled with a plethora of behavioural deficits are the symptoms of this disease. Being a degenerative disease, there is an increase in the severity of these symptoms as the disease progresses. Pathologically(Alzheimer, 1907), AD is characterized by the accumulation of Amyloid Beta (Aβ) plaques (Glenner and Wong, 1984; Masters et al., 1985) and neurofibrillary tangles (accumulation of τ-protein) in diseased brains(Goedert et al., 1988; Grundke-Iqbal et al., 1986; Ihara et al., 1986; Kosik et al., 1986). There are also other structural and functional changes that take place in the AD affected brain(Rozemuller et al., 1986; Wyss-Coray, 2006; Markesbery, 1997; McGeer et al., 2006). These pathological changes give rise to severe impairment of neuronal and synaptic function which in turn manifests itself as cognitive defects like memory loss (LaFerla et al., 2007).

The approach to tackling this issue has been to understand the molecular pathways involved in AD. One very crucial pathway involves the production of Amyloid Beta(Aβ). Aβ is produced by the cleavage of Amyloid Precursor Protein (APP), a protein abundantly expressed in various brain regions(Figure 2). APP, a trans-membrane protein containing a large extra cellular domain and a small cytoplasmic membrane, when cleaved sequentially by β-Secretase and γ-Secretase, results in the formation of Aβ. This pathway of sequential cleavage by β and γ-Secretase is called the Amyloidogenic pathway. APP can also be cleaved by α-Secretase, resulting in partial fragments of APP that cannot be further cleaved by γ-Secretase. The cleavage of APP that gives rise to fragments that cannot produce Aβ is called the Non-Amyloidogenic pathway (LaFerla et al., 2007). These reactions are listed in Figure 1.

It is important to note that the most prominent pathway for cleavage of APP is the Non-Amyloidogenic pathway (Kojro and Fahrenholz, 2005). However, despite the fact that only a subset of APP molecules undergo cleavage via the Amyloidogenic pathway, even in a healthy brain, a considerable amount of APP gets converted to Aβ that is secreted extracellularly. This Aβ produced in the healthy brain then gets cleared through a re-uptake mechanism that ensures that the Aβ does not aggregate to form plaques. The exact percentage of APP molecules undergoing cleavage via the two pathways is not known. In the diseased condition, one or more of these reaction's equilibrium gets perturbed, resulting in an accumulation of Aβ that the re-uptake mechanism is unable to clear, thus forming plaques.(Claeysen et al., 2012)

Mutations in APP and γ-Secretase have been known to cause Early-Onset AD (St George-Hyslop and Petit, 2005). These mutations either result in the overproduction of Aβ or affect the stability of Aβ that is formed. For example, one APP mutation called APP-Swedish results in greater cleavage of APP by β-Secretase as compared to wild-type APP (Haas et al., 1995). It has also been shown that patients affected with Down Syndrome, where there is a trisomy in chromosome 21 (APP is found on chromosome 21) show early accumulation of Aβ (Gyure et al., 2001; Mori et al., 2002).

As elaborated above, APP plays a crucial role in the production in Aβ. The aim of this

Non-Amyloidogenic pathway:

APP + α-Secretase   -> CTF-α

Amyloidogenic pathway:

APP + β-Secretase   -> CTF-β

Amyloid-β formation:

CTF-β + γ-Secretase -> Amyloid-β

Figure 1: APP is processed via two pathways. The Amyloidogenic and the Non-Amyloidogenic pathway. Processing by the Non-Amyloidogenic pathway happens more often when compared to the Amyloidogenic pathway. The product formed by the Non-Amyloidogenic pathway, CTFα does not undergo further cleavage by any other Secretase and therefore does not form Aβ. Sequential cleavage by β- and γ- Secretase constitutes the Amyloidogenic pathway as it eventually results the formation of Aβ

project was to study in detail the various molecular interactions involving APP and the secretases involved in the pathway that produces Aβ. While there has been extensive research implicating Aβ and plaques as having a crucial role in AD, there havent been detailed quantitative studies elaborating the role of APP in the production of Aβ.

1.1 Pathological signatures of APP

1.1.1 APP over-expression in synapses

Over expression of APP is a pathological condition that gives rise to Early-Onset AD(Rovelet-Lecrux et al., 2006; Cabrejo et al., 2006). APP is also over expressed genetically in mouse models to mimic AD conditions. Therefore, it is important to study the clustering properties of APP under wild type conditions and over-expressed conditions. In this project, we ask how the over expression of APP molecules affects its clustering properties in terms of number and size. These results are then used to make inferences on the differential rates of formation of Aβ under wild type and over expressed conditions.

1.1.2 Cleavage of APP by β-Secretase

As mentioned previously, it has been shown that in the APP-Swedish mutation, there is a greater affinity between the mutant-APP and β-Secretase as compared to wild type-APP and β-Secretase. This greater affinity implies that there will be a greater rate of formation of Aβ in the APP-Swedish mutation. We test this hypothesis using our model in this project. We also test the role clusters play when it comes to cleavage by β-Secretase molecules.
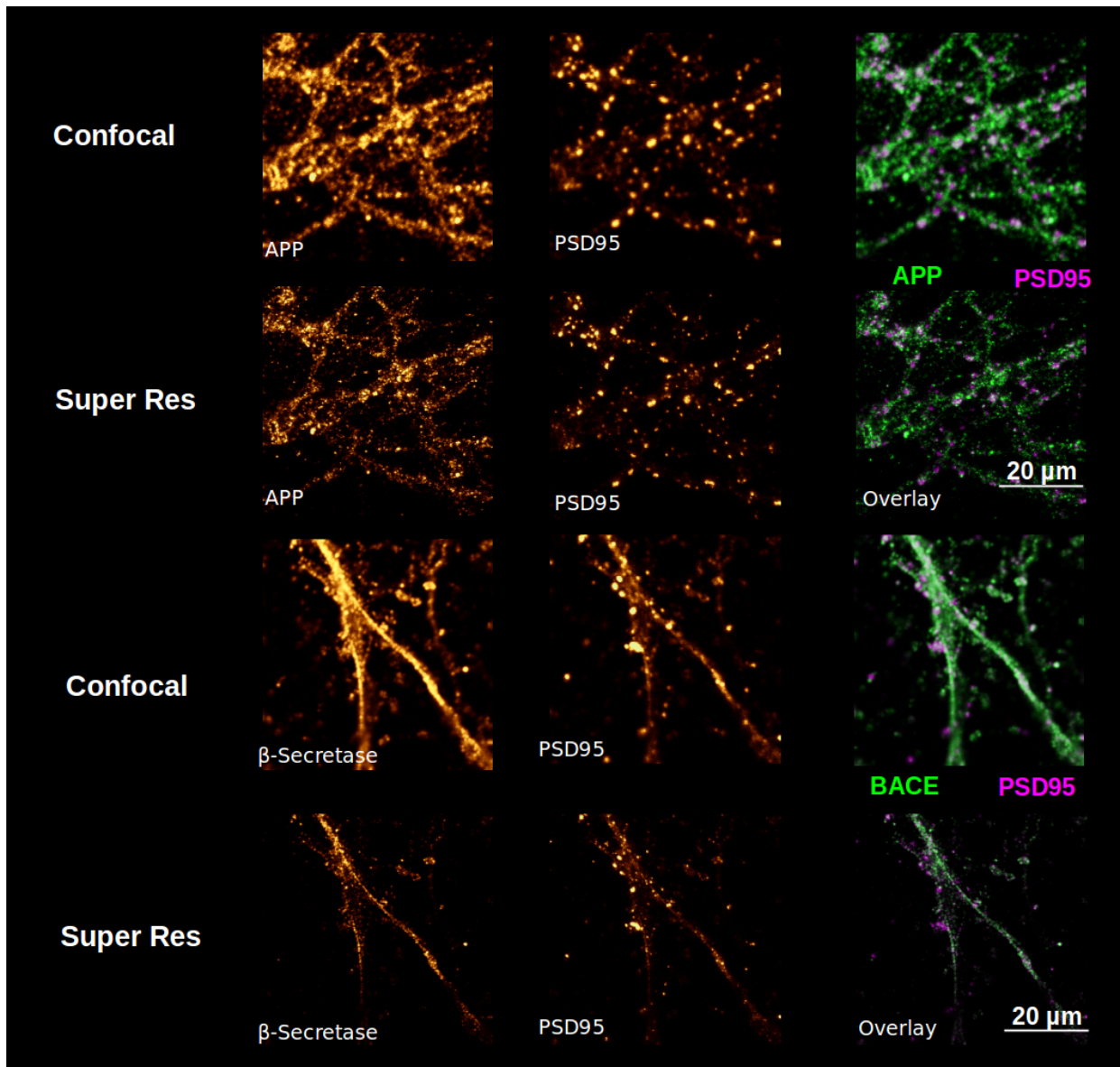
Figure 2: Visualization of APP and β-Secretase on Hippocampal neurons using Super-Resolution and Confocal Microscopy. Prior to the use of Super-Resolution microscopy, the distribution and localization of APP and β-Secretase could not be precisely quantified using Confocal microscopy (As evident from the two panels showing Confocal images). Using Super Resolution Microscopy techniques (above image uses STED), the APP localization is precisely quantifiable to the extent that APP monomers and clusters can be distinguished and counted with certainty. Using this rich STED Microscopy data, we build our model to mimic the clustering and localization in synapses. In these images, BACE indicates β-Secretase, PSD95 is a marker that helps in visualization of the Post-Synaptic Density. It is very evident from this image that APP is present throughout the all neuronal membranes and not just restricted to synapses. This image has been obtained from Kedia et al.(unpublished data) and reproduced with permission.

1.2   Insights from experimental data

With the help of Super-resolution microscopy, details about the properties of APP molecules on the post synapse were obtained by Deepak Nair's lab at IISc, Bangalore. They found that APP was abundantly present on the pre and post synapses in Hippocampal and Cortical slices. This has been previously reported widely in recent literature. However, it was also found that APP occasionally forms clusters that are relatively stationary on the synaptic membrane. This novel result was the motivation for modelling the clustering details of APP on the synapse (Kedia et al., unpublished).

APP forms clusters on the synaptic membrane

In AD, since plaques are found in the synapses that give rise to shrinkage and loss of synaptic boutons (Koffie et al., 2011), this project will focus on the presence of APP on synapses. The density of APP molecules present on the Peri-Synaptic and Post-Synaptic region of synapses has been shown in Figure 3. It is important to note that a Peri or Post Synaptic region is considerably smaller than a micrometer square in area. This density value represents all classes of APP molecules including monomers and clusters. It is also observed that there are a few APP clusters found per micrometer square of synaptic area. This is plotted in Figure 4 and Figure 5. Here, the definition of an APP cluster is a collective of 4 or more APP molecules bound together with a relatively low diffusion coefficient compared to the diffusion coefficient of the monomer. The total number of APP molecules seen per cluster is plotted in Figure 6 and Figure 7. This suggests that the APP clusters are relatively huge, which explains the low diffusion coefficient. The clustering properties of APP are extensively studied in this project and the role it may play the pathological formation of plaques is also discussed (Kedia et al., unpublished).
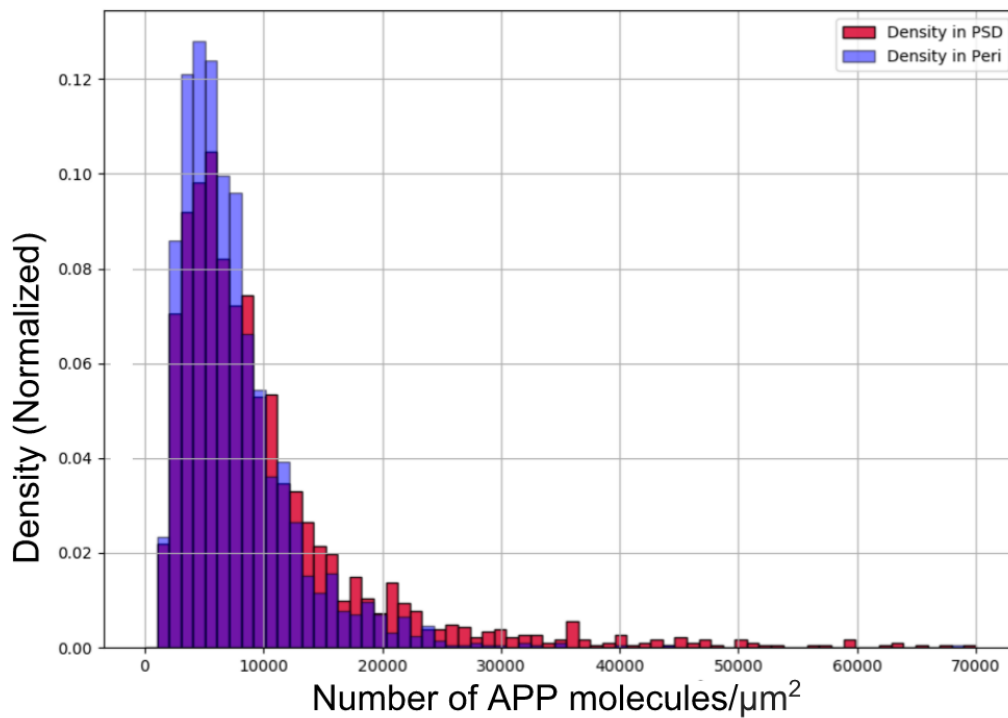
Figure 3: Normalized histogram of frequency of occurrence of various APP densities on Peri and Post synapse. The X-axis in this plot represents the APP density averaged after sampling all Post-Synaptic(Red histogram) and Peri-Synaptic(Blue histogram) surfaces on Hippocampal synapses. As evident from the plot, there are 1000s of APP molecules/μm^2 on a synaptic surface. It is important to note however that a Post Synaptic Density(PSD) or a Peri-Synapse is usually much smaller than 1 μm^2 in area. This data has been obtained from Kedia et al.(unpublished data) and reproduced with permission.
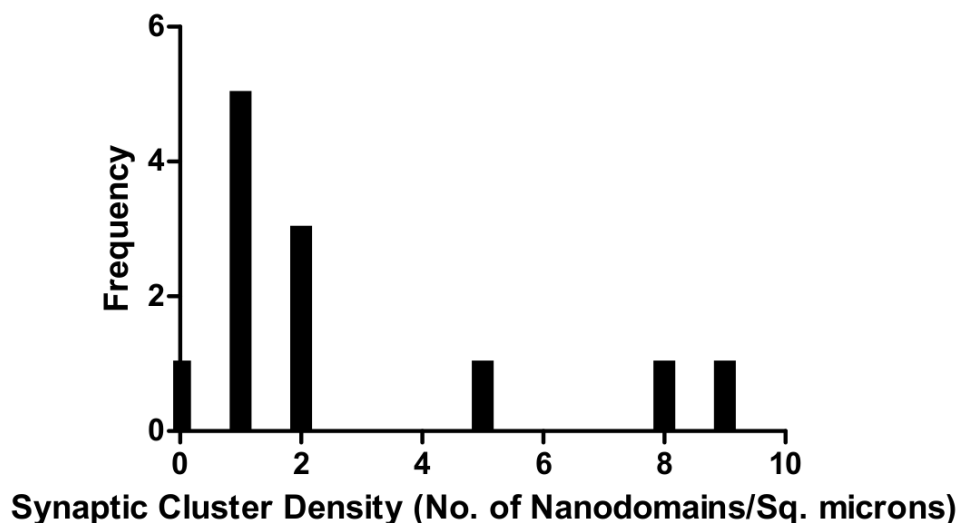
Figure 4: Plot of density of clusters formed in the Post Synapse per μm^2. As indicated earlier, a typical Post synapse is much smaller than 1 μm^2 and therefore, the interpretation of this figure is that most small synapses contain no clusters and few large synapses contain 1-3 clusters. In this figure, a nanodomain refers to APP clusters. This data has been obtained from Kedia et al.(unpublished data) and reproduced with permission.
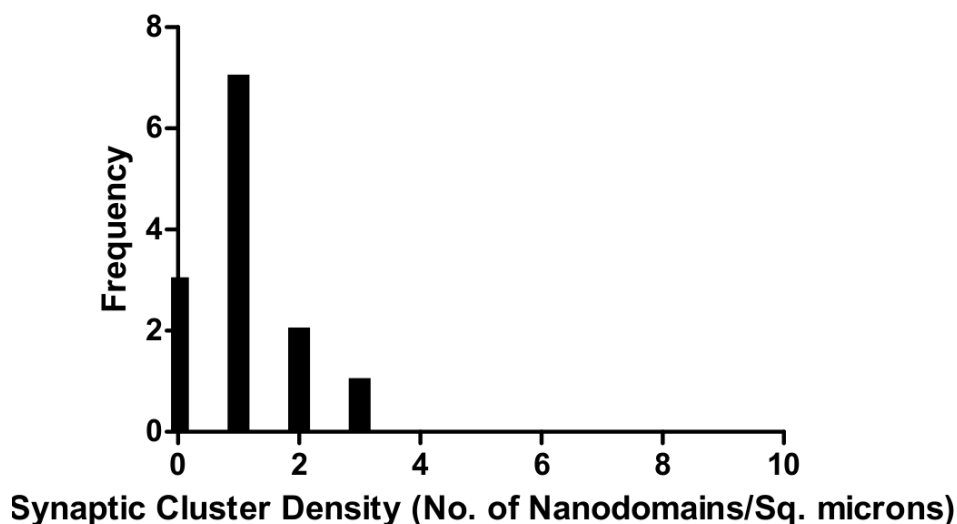
Figure 5: Identical plot as the previous figure for data from Peri Synapse. This data has been obtained from Kedia et al.(unpublished data) and reproduced with permission.
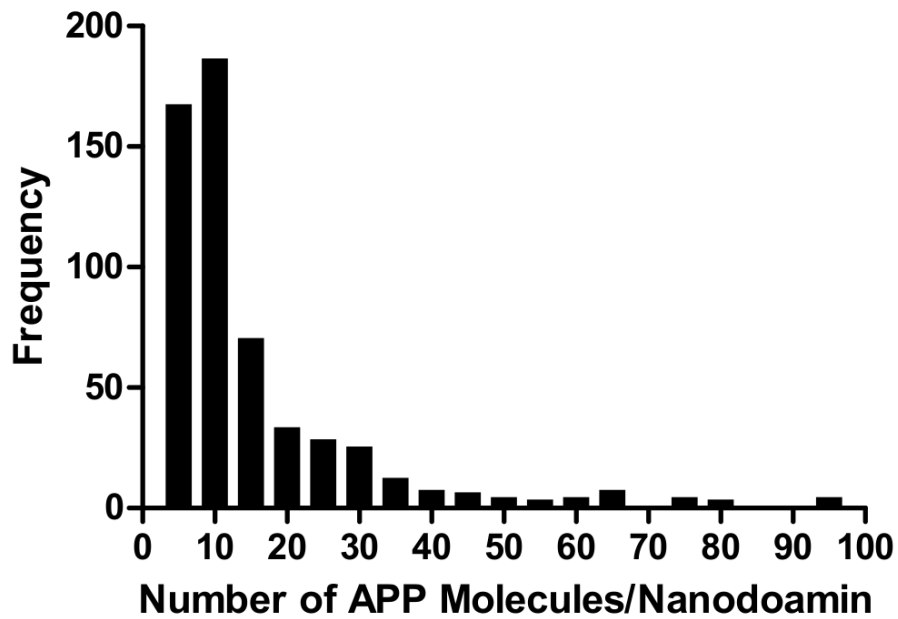
Figure 6: Plot of number of APP molecules per cluster in Post Synapse versus frequency of occurrence. This data has been obtained from Kedia et al.(unpublished data) and reproduced with permission.
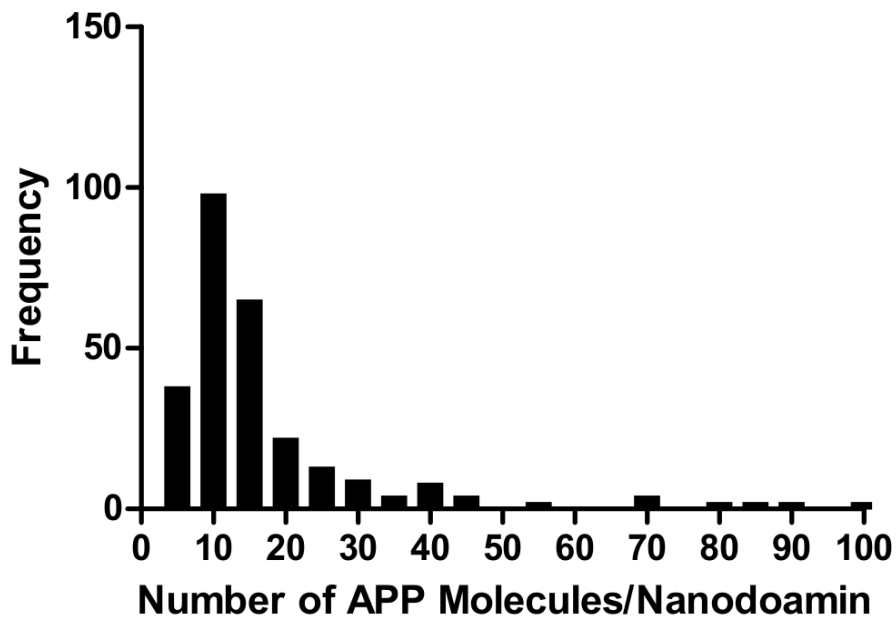
Figure 7: Plot of number of APP molecules present per cluster in the Peri Synapse versus the frequency of occurence. Identical to previous plot for data from Peri Synapse. This data has been obtained from Kedia et al.(unpublished data) and reproduced with permission.
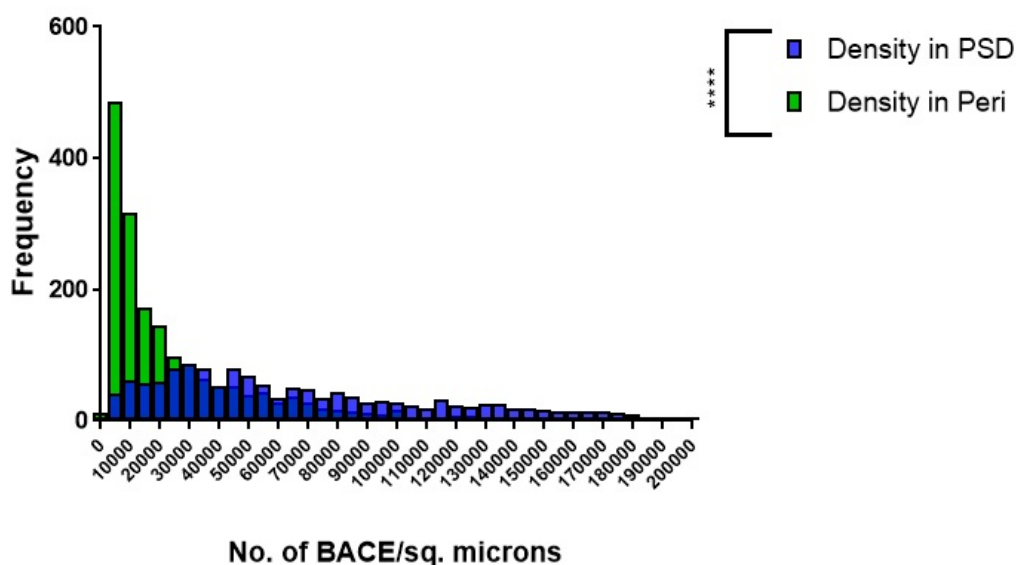
Figure 8: β-Secretase density on Post and Peri-synapse. As evident from figure, β-Secretase is present in excess when compared to the density of APP molecules. This data has been obtained from Kedia et al.(unpublished data) and reproduced with permission.
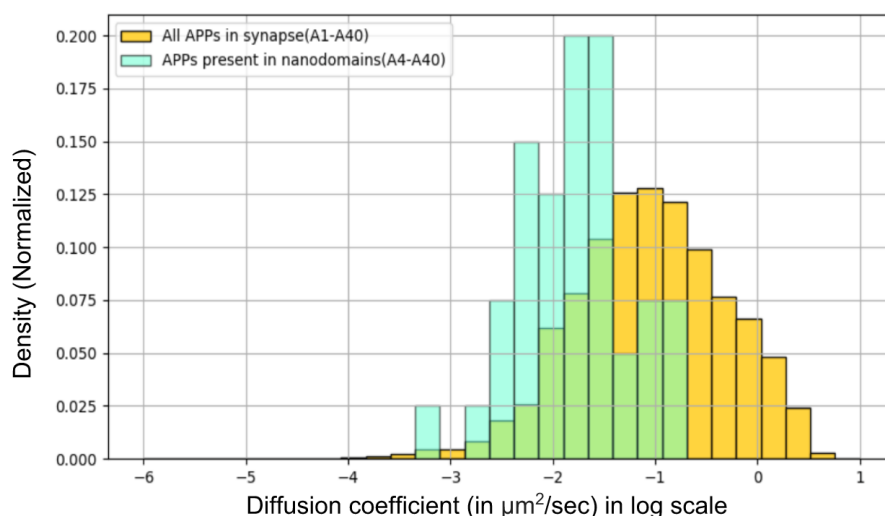
Figure 9: Experimentally observed diffusion coefficients for different APP species. The yellow histogram consists of diffusion coefficients of all APP species plotted in the log scale on the X-axis versus their normalized frequency of occurrence. This consists of APP monomers, dimers, trimers and clusters of all sizes. The green histogram is the plot of the diffusion coefficients of the APP clusters in log scale on the X-axis. The units for the diffusion coefficient is $\mu m^2/sec$. From this plot, we can see that the clusters have much lower diffusion coefficient when compared to APP monomers(the yellow histogram predominantly represents monomers as these are the most abundant species of APP. This data has been obtained from Kedia et al.(unpublished data) and reproduced with permission.

11

2 Methods and model building

APP and its various interactions

There are two different types of interactions involving APP that are studied in this project. The first type of interactions are interactions of APP molecules among themselves and the second type of interactions are the ones between APP molecules and the different Secretase molecules. In regard to the first type of interaction, APP is found in synapses in the form of monomers and clusters. The monomers have a relatively high diffusion coefficient as compared to the clusters. The interactions within the different types APP molecules is listed in Figure 10. Regarding interactions between APP molecules and Secretase molecules, in this project the only Secretase we study is β-Secretase. While β-Secretase has also been known to be present in cluster form, we assume that these clusters of β-Secretase are simply monomers of β-Secretase aggregating around clusters of other membrane proteins that β-Secretase interacts with. The interactions between the different APP species and β-Secretase has been elaborated in Figure 11.

$$A1 + A1 \rightleftharpoons A2 \; [k_1, k_{-1}]$$
$$A2 + A1 \rightleftharpoons A3 \; [k_2, k_{-2}]$$

$$A3 + A1 \rightleftharpoons A4 \; [k_3, k_{-3}]$$

$$A4 + A1 \rightleftharpoons A5 \; [k_4, k_{-4}]$$
$$A5 + A1 \rightleftharpoons A6 \; [k_5, k_{-5}]$$
$$....$$
$$A39 + A1 \rightleftharpoons A40 [k_{39}, k_{-39}]$$

   a. Fast diffusing   b. Interactions forming   c.   Nanodomain growth
          interactions   nanodomains
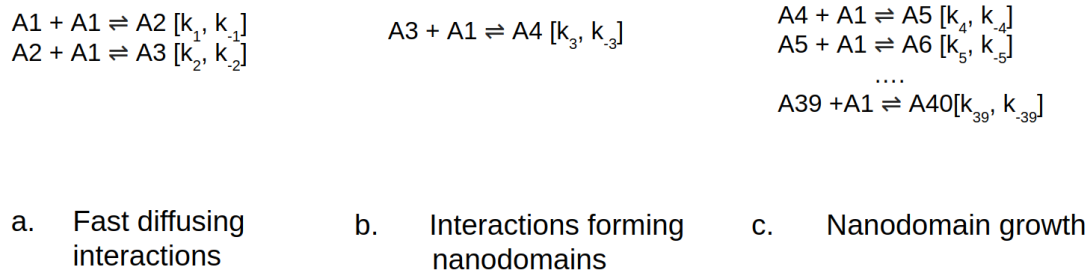
Figure 10: List of all possible types of interactions within the different APP species. These interactions are classified into three categories. **a**. Fast diffusing interactions that involve APP monomers. As the monomers have a high diffusion coefficient, these reactions happen in abundance. **b**. The reactions that give rise to formation of an APP cluster(or a nanodomain). The rates of this reaction combined with the fast diffusing interactions are heavily constrained in the model as the number of clusters formed are very precise. **c**. List of reactions that are involved in the growth of the nanodomain. We have limited the size of the cluster to 40 APP molecules for convenience as the distribution in Figure 6 and 7 have a long tail. The forward and backward rates of the reaction are indicated inside the brackets.

$$A1 + \beta\text{-Secretase} \;\longrightarrow\; P \qquad\qquad [k_{f1}]$$
$$A2 + \beta\text{-Secretase} \;\longrightarrow\; P + A1 \quad [k_{f2}]$$
$$....$$
$$A40 + \beta\text{-Secretase} \;\longrightarrow\; P + A39 \; [k_{f39}]$$

Figure 11: List of interactions between different APP species and β-Secretase. We assume that the reaction is unidirectional and cleavage by individual β-Secretase molecules happens sequentially. In this figure, P indicates the CTFβ that is formed by β-Secretase cleavage of APP.

2.1   Interactions between APP molecules to form clusters

It has been reported from the experimental studies that at steady state, there are around 6000-12000 APP monomers/μm^2 on the peri and post synapse. It has also been reported by the same study that there are around 0-10 clusters of APP /μm^2 and almost no dimers or trimers of APP/μm^2. This implies that at a time, there are a few thousand monomers of APP and a few clusters and on every Post Synaptic Density or Peri-Snaptic region, considering that these regions are well under 1 μm^2 in area. The diffusion coefficient for the APP monomer is also a few orders of magnitudes higher than that of the cluster (Kedia et al., unpublished).

The picture this paints is that there are abundant collisions between the thousands of fast diffusing APP monomers that occasionally polymerize to form a few stationary clusters.

This scenario is simulated in 3-D using MCell v3.4 (Stiles and Bartol 2001), a Monte-Carlo based simulation tool. To obtain the rates of the reactions in the Figure 10, 3000 APP monomers are released on a surface with suitable diffusion constant and allowed to collide with each other. Reaction rates are picked randomly for the reactions listed in Figure 10 and the rates that give rise to around 0-2 clusters and almost no dimers or trimers are selected. The selected rates are those rates that give rise to the steady state densities of the various APP species.

2.2   Interactions between APP and β-Secretase

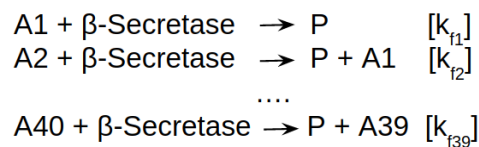The density of β-Secretase as observed from experiments range from 5000 - 50000 β-Secretase molecules/μm^2. For steady state cleavage of the various APP species, the different APP species are released from the surface with 14000 β-Secretase molecules (Kedia et al., unpublished). The interactions between APP and β-Secretase are listed in the Figure 11. There is no experimental estimate of the density of the product P of this reaction, which is C-terminal fragment β(CTFβ). Therefore, we try to compute the amount of C-terminal fragment β formed for different values of binding rates. The reaction rates for the cleavage of clusters of APP with β-Secretase is assumed to be proportional to the size of the APP cluster. The equation relating the reaction rate of cleavage for a cluster with the size of the cluster and the reaction rate of cleavage for a monomer is written below.

$$k_f^n = n^m \times k_f^1 \tag{1}$$

Here, k_f^n is the forward binding rate for β-Secretase with an APP cluster containing n APP molecules, k_f^1 is the forward binding rate for β-Secretase with an APP monomer, n is the number of APP molecules in the cluster and m is the coefficient for cooperativity. This cooperativity coefficient has been inspired by the Hill's coefficient (Hill 1910). The Hill's coefficient is usually used to model cooperative or non-cooperative binding of enzymes to complex receptor molecules depending on configuration and state of the receptor molecule. As the reaction being modelled above does not exactly fall in the category of those reactions modelled by the Hill equation, we refer to the coefficient m as the cooperativity coefficient.

The justification for using this relation is as follows. It has been demonstrated in some polymers that it is possible to have a binding rate non-linearly proportional to the size of the polymer (Westmeyer et al., 2004). Since the relation between binding rate with β-Secretase and the size of the APP cluster is unknown, we perform the simulation for multiple values of m. For a value m = 1.0, it means that the attractive interactions between an APP cluster of size n and β-Secretase is similar to if there were n monomers of APP. For a value m > 1.0, it means that the affinity between an APP cluster of size n and β-Secretase is greater than the affinity of n individual monomers of APP with β-Secretase. For a value m < 1.0, it means that the affinity between an APP cluster of size n and β-Secretase is lesser than the affinity of n individual monomers of APP with β-Secretase.

2.3 Modelling the canonical Peri-Synaptic surface using MCell

2.3.1 Formation of APP clusters

We model a rectangular surface of dimensions $0.6\mu m \times 0.6\mu m$. The dimensions of this surface are taken to roughly mimic one Peri-Synaptic region. Primarily, the cleavage of APP by β-Secretase happens at the Peri-Synapse and hence the choice to model the surface as a canonical Peri-Synapse. To this canonical Peri Synaptic Density with area 0.36 μm^2 we assume that at steady state, there will be a total of 3000 APP molecules, mostly as monomers, almost no dimers and trimers and around 0-2 clusters of APP. These numbers are picked roughly from the experimental results. The diffusion constant for the APP monomer is taken to be 4.0×10^{-9} μm^2/sec and that of the APP cluster is 2.5×10^{-10} μm^2/sec.

2.3.2 Studying β-Secretase cleavage of APP

We take the same rectangular surface of dimensions 0.6 $\mu m \times 0.6 \mu m$. To this canonical Peri Synaptic Density with area 0.36 μm^2 we assume that at steady state, there will be 1180 APP monomers, no dimers and trimers and 1 cluster of APP containing 20 APP molecules. The justification for the reduced density of APP on this canonical surface as compared to the previous canonical surface is that a subset of APP molecules are unavailable for cleavage by β-Secretase because they have already been cleaved by other enzymes on the surface.

While modelling the surface with β-Secretase, the number of β-Secretase molecules for the surface is taken to be 14000. The listed number of molecules are released on the surface and linear or non-linear binding rates are picked for the reactions. Then, the number of product molecules formed for these respective rates is counted.

3 Results

3.1 Constraining rates prior to obtaining experimental data on dimer and trimer density

Originally, the experimental data obtained by Kedia et al.,(unpublished data) consisted of APP density data for clusters of APP and all APP species. The APP cluster density was sufficiently detailed in terms of representing the properties of APP aggregates containing 4 or more APP molecules. The density of all APP molecules, which was calculated by measuring the total intensity of APP on synapses divided by the intensity of an APP monomer, represented all the APP species including monomers, dimers, trimers and clusters. By subtracting the density of clusters from the density of all the APP species, the density of monomers, dimers and trimers put together was obtained. As this data represented monomers, dimers and trimers, it was impossible to strictly constrain the binding rates for the reactions listed in Figure 10. The range of binding rates that fit the experimental data was so large that it indicated that there was a lack of sufficient experimental data to succesfully model these reactions.

This detail was subsequently pointed out to Kedia et al. and the data for the densities of monomers, dimers and trimers were separately analyzed. It was after this second round of analysis prompted by the model that the densities were seperately obtained. It was found that there are almost no dimers and trimers on the synaptic membranes. The details of these densities are plotted in Figure 12 and Figure 13. We therefore conclude that most of the APP molecules are present as monomers, with a few clusters also present.
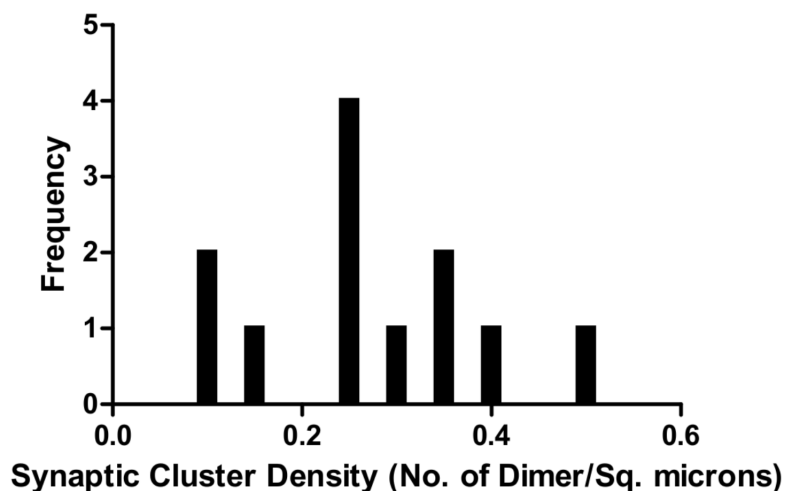

Figure 12: Plot of density of dimers formed in the Post Synapse per μm^2. As indicated earlier, a typical Post synapse is much smaller than 1 μm^2 and therefore, the interpretation of this figure is that no dimers seen on synaptic surfaces. This data has been obtained from Kedia et al.(unpublished data) and reproduced with permission.
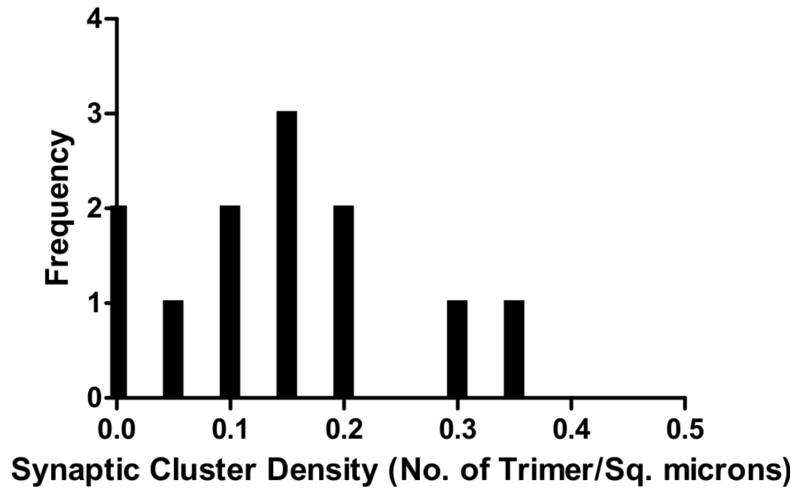
Figure 13: Identical plot as the previous figure for data for trimers in the Post Synapse per μm^2. The interpretation for this data is that there are almost no trimers in an ideal Post Synaptic membrane. This data has been obtained from Kedia et al.(unpublished data) and reproduced with permission.

3.2 Obtaining steady state binding rates using analytical methods

As a comparison to the rates obtained by the MCell simulations, the exact equations were also modelled analytically. The rate of production of the product was set to zero to mimic the steady state concentrations of each species and the rates obtained were compared to the rates observed after the MCell simulations.There were minute differences between the two sets of rates obtained but the rates obtained analytically reaffirmed that the MCell reaction rates were accurate. The differences between the rates could be explained by the drawbacks of the analytical method.

The reasons for using MCell simulations over the steady state ODE solutions are numerous. Primarily, the analytical solution assumes that there are plenty of interactions between all the different types of molecules present. This assumption cannot be justified under conditions where there are molecules with low diffusion coefficients and therefore have different rates of encounter compared to fast diffusing molecules. There is also the constraint of geometry that is an important detail while modelling synaptic surfaces. The diffusing molecules are restricted by the complex geometrical shapes of the surface and in the future, we plan to use a synaptic reconstruction model. We therefore proceed with only the MCell model and use the analytical model as a reference to validate the rates obtained from the MCell simulations.

3.3 Computational modelling of APP over-expression studies

Over-expression of APP molecules has been frequently used in mouse models to produce Aβ plaques mimicking Alzheimers disease. APP over-expression under pathological conditions can also be a cause of Early Onset-AD like in Down Syndrome, where there is a trisomy of Chromosome 21 which has the APP gene. Therefore, we use our model to study the dynamics of APP cleavage under over-expression conditions. However, to obtain the APP clustering dynamics with over-expressed APP, it is first

necessary to study the clustering dynamics under healthy conditions. With the help of experimental data on the steady-state sizes of clusters under healthy conditions, we calculate the binding rates for interactions among the different APP species.

3.3.1 Constraining reaction rates for APP clustering in healthy synapses

As elaborated in the methods section, there are around a few thousand APP monomers on a synaptic surface(PSD or Peri), almost no dimers and trimers and around 0-2 clusters. The diffusion coefficients for the monomers are relatively high compared to the clusters. Therefore, among the abundant collisions taking place between these different species of APP, occasionally the size of the APP species grows or reduces as a result of a collision or a dissociation event. These instantaneous reactions can be modelled as the set of equations shown in Figure 10.

To details of how these rates were obtained are in the methods section The rates were selected such that less than 2 clusters are produced. The rates obtained for these reactions are listed in table

3.3.2 Increasing expression of APP molecules results in excessive increase of APP clusters

With the set of reaction rates shown in Table 1, APP was over-expressed on the membrane by releasing 6000 monomers instead of 3000. The amount of clusters formed for an instantiation of 6000 monomers was counted for identical simulation time. This is represented in Figure 14. From this figure, it is evident that by doubling the number of monomers, there's a multi-fold increase in the number of clusters formed. The variation in the data arises from the variation in the reaction rates used for this simulation. A range of reaction rates(as shown in table) satisfied the condition of forming at most 2 clusters with almost no dimers or trimers. This same range of reaction rates were used in the over-expression condition to count the number of clusters. Therefore, the range of values represents a loose constraining in terms of modelling done to avoid over-fitting to the experimental data. Therefore it is inappropriate to do any form of statistics on this data set as the variation carries meaningful information.

The model therefore predicts the amount of clusters that would be formed if APP was over-expressed in the Peri-Synaptic region. This non-linear increase ensures that even if β-Secretase preferentially cleaved only APP clusters(with a high value for the coefficient m) and was agnostic to the number of APP monomers present in the membrane, there would still be an overproduction of Aβ if APP was over-expressed.

17

Reaction	Forward Rate(k_f) in $\log_{10}$ scale (units for forward rate is $\mu m^2 s^{-1} molecules^{-1}$)	Backward Rate(k_b) in $\log_{10}$ scale (units for backward rate is s^{-1})	Equilibrium constant(K_{eq}) in $\log_{10}$ scale (units for equilibrium rate is $\mu m^2 molecules^{-1}$)
A1 + A1 $\rightleftharpoons$ A2	(-5.8) - (-3.0)	(2.0) - (5.0)	(-8.0) - (-7.7)
A2 + A1 $\rightleftharpoons$ A3	(-2.7) - (-1.6)	(2.2) - (3.0)	(-5.0) - (-4.5)
A3 + A1 $\rightleftharpoons$ A4	(-2.3) - (1.9)	(2.0) - (5.8)	(-5.0) - (-3.0)
A4 + A1 $\rightleftharpoons$ A5	(0.0) - (1.9)	-2.0	(-2.0) - (-0.1)
A5 + A1 $\rightleftharpoons$ A6	(0.4) - (2.1)	-2.0	(-1.6) - (0.1)
A6 + A1 $\rightleftharpoons$ A7	(1.8) - (2.4)	-2.0	(-0.2) - (0.4)
A7 + A1 $\rightleftharpoons$ A8	(1.0) - (2.2)	-2.0	(-1.0) - (0.2)
A8 + A1 $\rightleftharpoons$ A9	(0.3) - (2.2)	-2.0	(-1.7) - (0.2)
A9 + A1 $\rightleftharpoons$ A10	(-0.3) - (2.0)	-2.0	(-2.3) - (0.0)
A10 + A1 $\rightleftharpoons$ A11	(-0.3) - (1.9)	-2.0	(-2.3) - (0.1)
A11 + A1 $\rightleftharpoons$ A12	(-0.8) - (1.7)	-2.0	(-2.8) - (-0.3)
A12 + A1 $\rightleftharpoons$ A13	(-1.9) - (1.4)	-2.0	(-3.9) - (-0.6)
A13 + A1 $\rightleftharpoons$ A14	(-2.0) - (1.3)	-2.0	(-4.0) - (-0.7)
A14 + A1 $\rightleftharpoons$ A15	(-2.1) - (1.1)	-2.0	(-4.1) - (-0.9)
A15 + A1 $\rightleftharpoons$ A16	(-2.2) - (0.9)	-2.0	(-4.2) - (-1.1)
A16 + A1 $\rightleftharpoons$ A17	(-2.2) - (0.9)	-2.0	(-4.2) - (-1.1)
A17 + A1 $\rightleftharpoons$ A18	(-2.2) - (0.9)	-2.0	(-4.2) - (-1.1)
A18 + A1 $\rightleftharpoons$ A19	(-2.5) - (0.5)	-2.0	(-4.5) - (-1.5)
A19 + A1 $\rightleftharpoons$ A20	(-2.5) - (0.4)	-2.0	(-4.5) - (-1.6)
A20 + A1 $\rightleftharpoons$ A21	(-2.8) - (0.3)	-2.0	(-4.8) - (-1.7)
A21 + A1 $\rightleftharpoons$ A22	(-3.1) - (0.0)	-2.0	(-5.1) - (-2.0)
A22 + A1 $\rightleftharpoons$ A23	(-3.1) - (-0.2)	-2.0	(-5.1) - (-2.2)
A23 + A1 $\rightleftharpoons$ A24	(-3.8) - (-0.5)	-2.0	(-5.8) - (-2.5)
A24 + A1 $\rightleftharpoons$ A25	(-4.0) - (-1.0)	-2.0	(-6.0) - (-3.0)
A25 + A1 $\rightleftharpoons$ A26	(-4.1) - (-1.0)	-2.0	(-6.1) - (-3.0)
A26 + A1 $\rightleftharpoons$ A27	(-4.2) - (-1.2)	-2.0	(-6.2) - (-3.2)
A27 + A1 $\rightleftharpoons$ A28	(-4.5) - (-1.5)	-2.0	(-6.5) - (-3.5)
A28 + A1 $\rightleftharpoons$ A29	(-4.6) - (-1.9)	-2.0	(-6.6) - (-3.9)
A29 + A1 $\rightleftharpoons$ A30	(-4.6) - (-1.9)	-2.0	(-6.6) - (-3.9)
A30 + A1 $\rightleftharpoons$ A31	(-5.0) - (-2.0)	-2.0	(-7.0) - (-4.0)
A31 + A1 $\rightleftharpoons$ A32	(-5.2) - (-2.3)	-2.0	(-7.2) - (-4.3)
A32 + A1 $\rightleftharpoons$ A33	(-5.2) - (-2.5)	-2.0	(-7.2) - (-4.5)
A33 + A1 $\rightleftharpoons$ A34	(-5.3) - (-2.7)	-2.0	(-7.3) - (-4.7)
A34 + A1 $\rightleftharpoons$ A35	(-5.3) - (-2.8)	-2.0	(-7.3) - (-4.8)
A35 + A1 $\rightleftharpoons$ A36	(-5.4) - (-2.9)	-2.0	(-7.4) - (-4.9)
A36 + A1 $\rightleftharpoons$ A37	(-5.7) - (-3.8)	-2.0	(-7.7) - (-5.8)
A37 + A1 $\rightleftharpoons$ A38	(-5.9) - (-4.2)	-2.0	(-7.9) - (-6.2)
A38 + A1 $\rightleftharpoons$ A39	(-6.0) - (-4.5)	-2.0	(-8.0) - (-6.5)
A39 + A1 $\rightleftharpoons$ A40	(-6.0) - (-5.1)	-2.0	(-8.0) - (-7.1)

Table 1: Rates for reactions in Figure 10
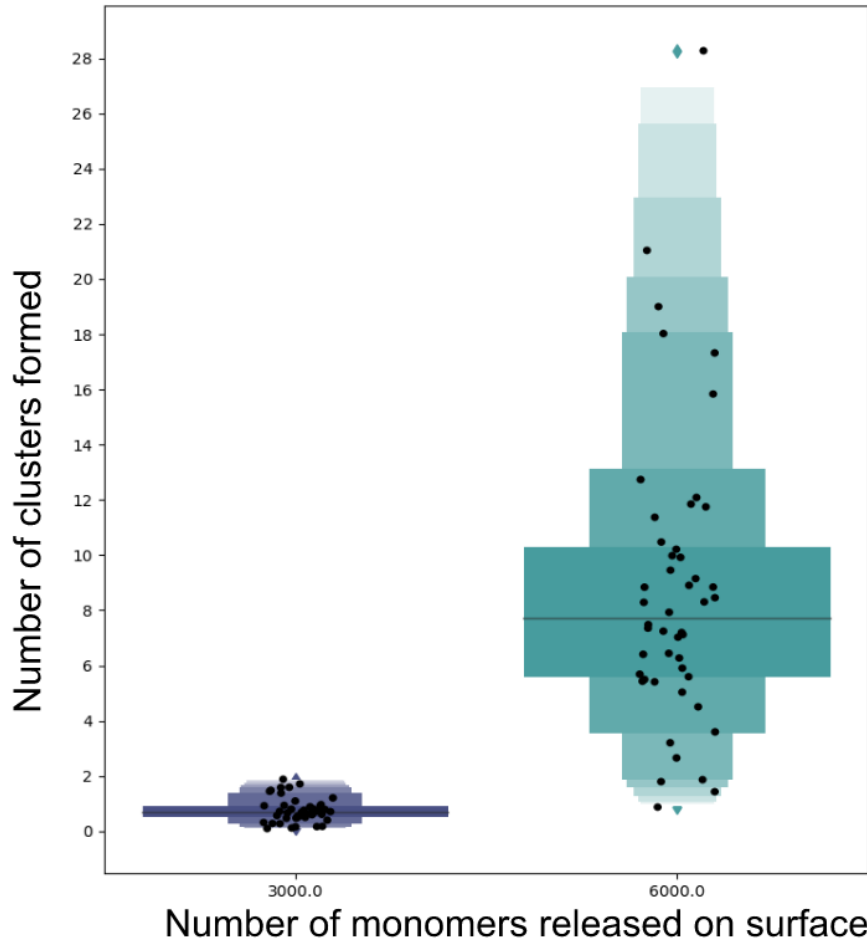
Figure 14: Number of clusters formed for normal vs over-expression of APP monomers. In this figure, while expressing 3000 molecules(left side of plot) on the surface (corresponds to a density of 8000 APP molecules/μm^2), we select those reaction rates that result in the production of around 0-2 clusters (corresponds to 0-7 clusters/μm^2). Each black dot on the graph represents one unique set of rates that were used to produce the said amount of clusters. In total, we have used 48 sets of reaction rates, with minute variations in each set. These 48 sets of reaction rates were then used(right side of plot) to simulate cluster formation for 6000 APP molecules on the surface(corresponding to 16000 APP molecules/μm^2). For double the number of monomers, we see around 10-fold increase in the number of clusters formed.

3.4   Implications of APP clustering

The first question that this project addresses is the role clustering of APP plays. It is evident from experimental data that APP forms clusters. But from a modelling perspective, it is important to ask whether it is necessary to model the detailed clustering interactions of APP. If the interactions between the APP and β-Secretase were identical regardless of whether the APP interacting was present as a cluster or a monomer, then the details about the clustering could be abstracted out and a model with uniformly distributed monomers would suffice. This is the first issue being investigated in this project.

Using the canonical peri-synapse, we ask if there would be any differences if the APP was present as clusters or just monomers. As control, we release 1200 monomers of APP along with 14000 β-Secretase molecules on the surface. As a comparison to this control, we release 1180 monomers of APP, one cluster containing 20 APP molecules and 14000 β-Secretase molecules on a similar surface. We then count the number of product molecules formed in both cases and compare the differences between the control and the case with the cluster.
For the binding rates, we use the identity in equation (1) to calculate the forward rates of the reactions listed in Figure 11. Three different values for the coefficient m are used (1.0,1.5 and 2.0). As evident from Figure 15, a coefficient of 1.0 produces marginally lesser or almost no different number of product molecules as compared to the control condition and a coefficient of 2.0 produces excess of product molecules as compared to the control conditions.

The conclusion from Figure 15 is that APP clusters produce a greater or lesser number of product molecules depending on the value of the coefficient m. Therefore, depending on the value of this coefficient, the decision of whether or not the clustering details should be abstracted out must be taken. At this stage, there is a lack of experimental evidence to conclusively arrive at what the value of the coefficient m should be. Therefore, we continue further modelling while keeping the coefficient m as an open parameter.
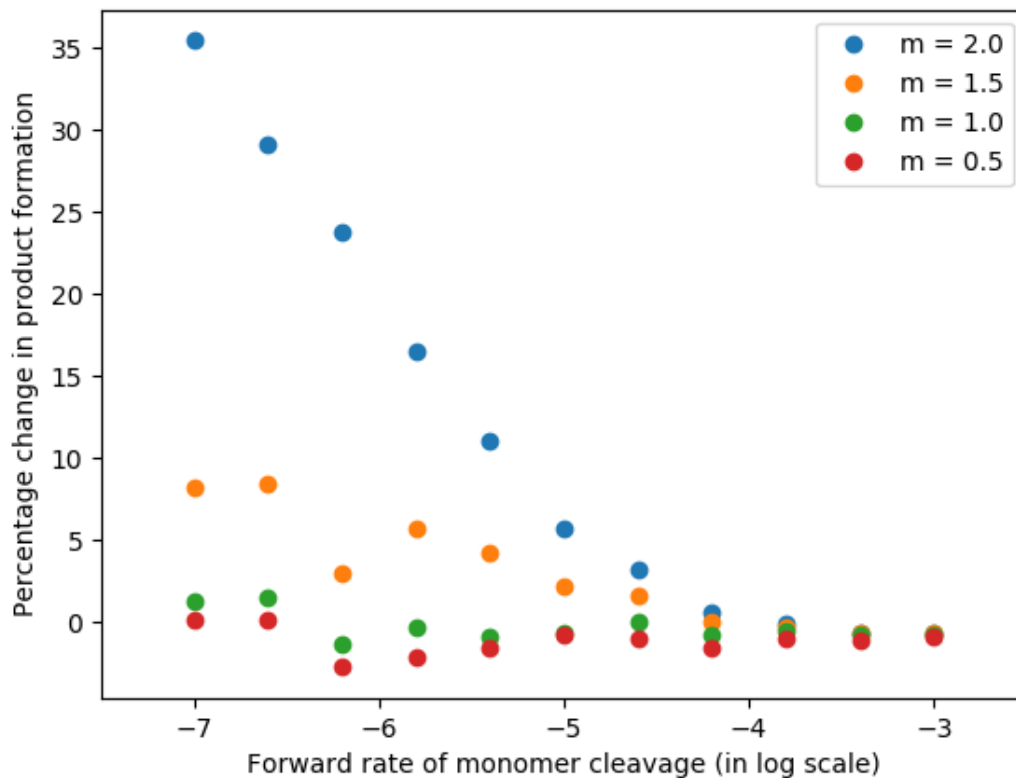
Figure 15: Percentage of product formed for reaction between APP with clusters and β-Secretase as compared to without clusters. We plot the percentage increase product formed(CTFβ) for different values of the coefficient m from equation (1). To calculate the percentage change, the amount of product(CTFβ) formed in the presence of 1 APP cluster of size 20 is compared to the amount of product(CTFβ) formed with only monomers present on the surface. For values of m = 2.0 and m = 1.5, we see that the scenario with clusters produces more product molecules than in the control scenario. For values of m = 1.0 and m = 0.5, we see that the scenario with clusters produces lesser or similar number of product molecules than in the control scenario. The inference from this plot is that depending on the coefficient m (or the differential affinity of β-Secretase to an APP cluster vs APP monomer), the percentage contribution to production of CTFβ from clusters to monomers varies according to the plot. If m was high, that would imply that β-Secretase primarily cleaves APP clusters and is agnostic to the amount of APP monomers present. If the value of m was low, this implies that CTFβ is formed from cleavage of both monomers and clusters.

3.5 Rate of cleavage for increased β-Secretase affinity

As mentioned previously, affinity of APP to β-Secretase is increased in the APP-Swedish mutation. Therefore, to test out the regimes of rate constants in which this increased rate constant will give rise to an increased production of product formed(CTFβ). This relation is plotted in Figure 16. Here, the number of product molecules formed is plotted for a given rate of monomer cleavage by β-Secretase. This plot is obtained from the same simulation set that studied the β-Secretase cleavage of APP(Methods section 2.3.2). As the total number of molecules released is 1200, the graph saturates at a value of 1200 for very high forward rate. For low forward rate of binding, there is a slight increase in the amount of product produced. While this increase may seem small in the graph, it is important to note that the timescale of the simulation being too less might be hiding the importance of this result. In the healthy brain, the time scales involved in the production and clearance of Aβ are unknown. There might be really fast production and really fast clearance or really slow production and clearance of Aβ. If it was the case that there is a really slow production and clearance rate of Aβ, then any minute increase in the amount of production of Aβ(via an increase in production of CTFβ) in this case could result in pathological formation of plaques. Therefore, the lower rates where only a minute increase in product is seen should not be ingnored.
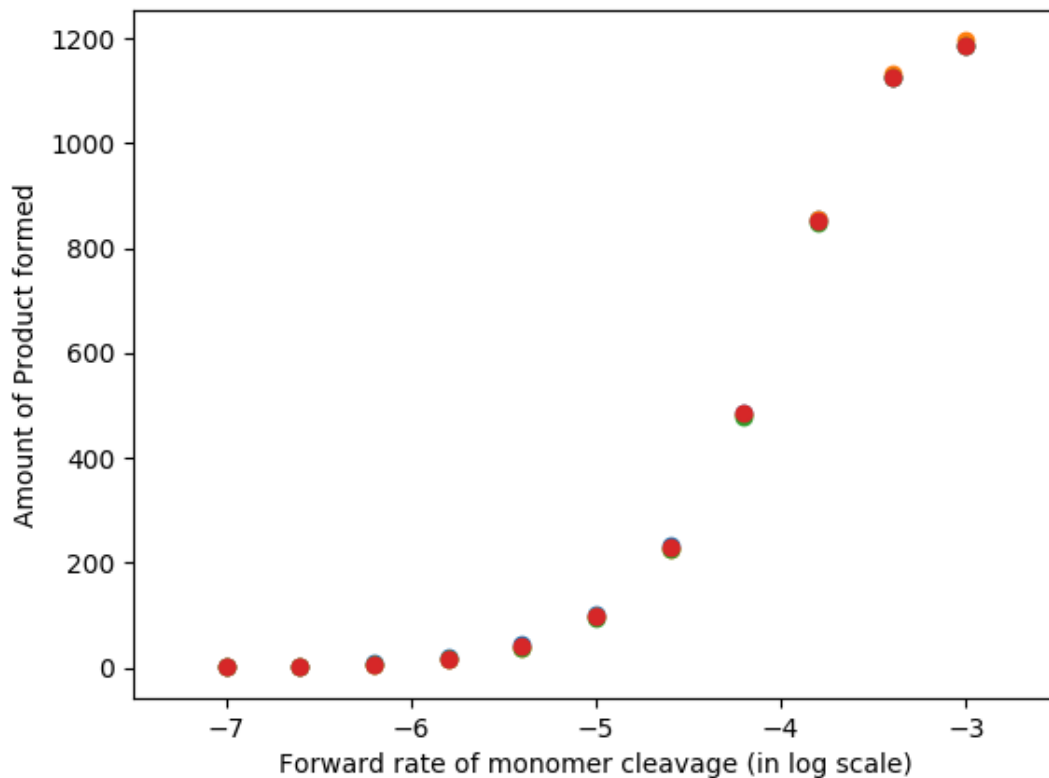
Figure 16: Number of product molecules formed for varying β-Secretase affinity. This is restricted to a fixed simulation time. The interpretation of this plot is that for a fixed time window, if the affinity to β-Secretase was increased,there would be a change in product molecules produced as shown in the figure. As evident from figure, the graph saturates(total APP molecules was 1200) for very high affinity rates and therefore, any increase in affinity will not result in an increase in products. For very low reaction rates, for the given simulation time there is very little increase in product formed. However it is important to note that we do not have an accurate estimate of the $in-vivo$ production time of CTFβ. Therefore, if our simulation time was to be increased, there would be a much higher increase in production of product molecules for increase in affinity rate in the lower spectrum of values. That is, there would be a steeper increase in the Y-axis values for the lower spectrum of X-axis values.

4 Discussion

A variety of pathological defects can show symptoms of Alzheimers disease. Mutations in the APP gene or improper regulation of APP gives rise to pathological formation of plaques. This accounts for a fraction of the cases of AD. Even in AD cases not involving pathology in interactions and production of APP, a detailed understanding of all the APP interactions can be used to regulate the formation $A\beta$. This is because APP cleavage by β-Secretase is the penultimate step in the formation of $A\beta$. Studying the interactions of APP is therefore a very relevant problem in relation to Alzheimers Disease.

This project deals with the role of clustering of APP molecules on Hippocampal synapses. As discussed earlier, APP is abundantly found on membranes of Hippocampal and Cortical neurons. Kedia et al. observed that APP is not just abundantly found but also forms clusters. This observation is the first time the clustering of APP has been quantified in detail. As the model we have built in this project uses data from Kedia et al., it discusses ideas about clustering of APP that have not been rigorously discussed in earlier literature. Therefore, the results discussed in this project are of paramount importance as the methods used here, detailed quantitative imaging combined with computational modelling are used to ask unique questions about the role of APP in the production of $A\beta$. It is important to note that this project only deals with the interactions of APP and does not quantitatively model the reactions resulting in the formation of $A\beta$. We therefore do not comment on the formation of $A\beta_{40}$ vs $A\beta_{42}$ nor do we comment on how $A\beta$ interactions give rise to plaque formation.

Even though clusters are shown to be present, it need not imply that APP on synapses with clusters is processed differently when compared to APP on synapses without clusters. We did not obtain any insights regarding this detail from previous literature or the experimental data provided by Kedia et al. Therefore, we felt it was important to address this issue before proceeding with the details of APP clustering. We used a relation (shown in Eqn 1) to simulate all possible types of differential interactions between APP clusters and β-Secretase. This relation was adapted from the Hill equation, an equation used in biochemistry that is used to model cooperative or non-cooperative binding in enzyme-substrate interactions. We show that for certain values of the coefficient (m=1), the interactions between the APP cluster (of size n) and β-Secretase molecules are identical to the case where there are n monomers of APP interacting with β-Secretase. For some values of the coefficient (m=1.5, 2.0), we see that the APP cluster produces more product molecules than n APP monomers. We also see that for m = 0.5, the number of product molecules produced with an APP cluster is lesser than the number of product molecules if all the APP molecules were uniformly distributed as monomers on the surface. The inference from this result is that the differential role that APP clusters play depends just on the coefficient of cooperativity in relation to β-Secretase cleavage. When the value of this coefficient is experimentally obtained, we will be able to determine whether APP clusters produce more or lesser $A\beta$ when compared to monomers using our model.

As β-Secretase has greater activity in endocytotic vesicles due to the lower pH, it is known that APP cleavage by β-Secretase happens in these vesicles under the synaptic

24

membrane (HS Ben et al., 2016). Our model is only a surface model and does not account for the production of CTFβ in these vesicles. When we discuss the product that is formed during APP cleavage by β-Secretase in this project, this product is primarily a proxy to represent this reaction happening inside vesicles. The product is therefore merely a readout and should not be considered literally as CTFβ. The exact details of this vesicular cleavage will be modelled shortly in this project. A representation of how APP clusters are distributed on vesicles is shown in Figure 17.
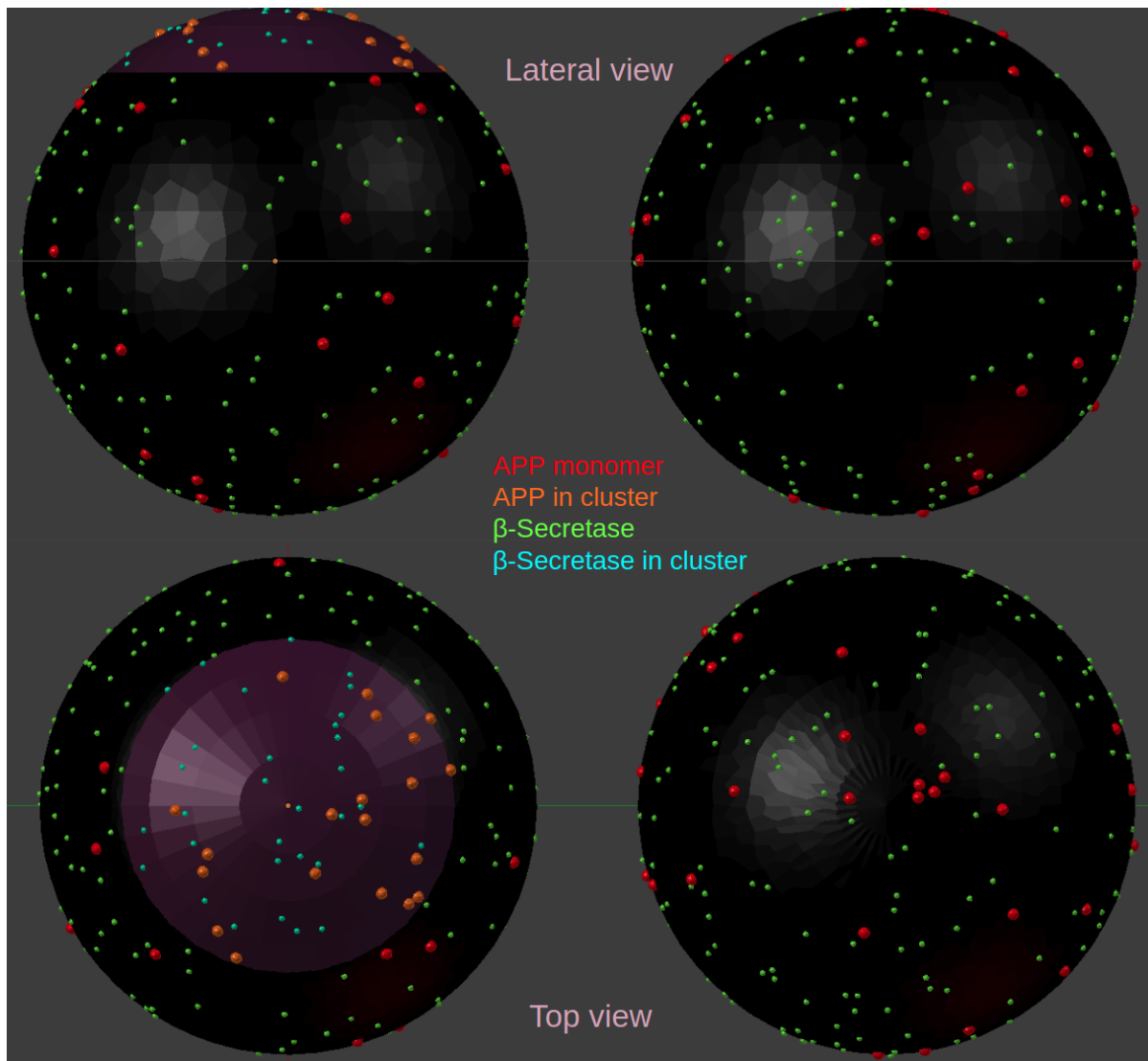
Figure 17: Spatial geometry of APP and β-Secretase distributed on an endocytic vesicle. Endocytic vesicles usually have a diameter of 40-150 nanometers. As the area of an APP cluster is as large as the total area of a small vesicle, we assume that only large vesicles contain clusters. The vesicles shown in this figure have a diameter of 120 nanometers. The vesicle on the left contains a single APP cluster along with a β-Secretase cluster co-localized to the same region. The area of the APP cluster(violet region) is $0.006 \mu m^2$ (matching with experimental cluster size). These vesicles are used to test the hypothesis whether APP clusters have a different rate of downstream processing when compared APP monomers present in vesicles.

$$\text{APP + BACE-1} \rightleftharpoons \text{intermediate } [k_1, k_{-1}]$$

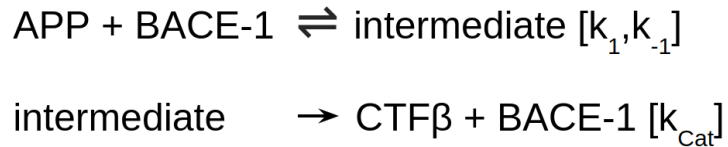$$\text{intermediate} \rightarrow \text{CTF}\beta \text{ + BACE-1 } [k_{Cat}]$$

Figure 18: Equations representing β-Secretase cleavage of APP if the reaction followed Michaelis-Menten kinetics with one intermediate

After discussing the role of APP clustering, we go on to model the details of the APP clusters with quantitative rigour using the experimental data provided. We successfully obtain interaction rates between the individual species of APP using MCell. Using these rates, we predict the number of clusters formed for the over-expression of APP. Our predictions suggest that there is a 10-fold increase in the number of clusters if the number of monomers on the surface are doubled. This prediction will be useful under the circumstance that β-Secretase has a very high preference for the cleavage of APP clusters and very low preference for APP monomers (seen when coefficient m=2.0). If this is indeed true (m=2.0), our model shows that there is indeed a much higher presence of clusters in the over-expressed condition that will therefore produce an excess of Aβ.

The model also tries to reproduce what happens if the affinity of APP to β-Secretase was increased. We systematically predict the increase in the amount of CTFβ formed for an increase in APP cleavage rate by β-Secretase. The motivation to model this was to study the repercussions of the APP-Swedish mutation, where there is an increased affinity for β-Secretase cleavage.

In conclusion, this project investigates the implications of each of the experimental observations(Kedia et al., unpublished) using a spatially realistic computational framework in regard to APP and its interactions with β-Secretase. Using this framework we have arrived at affinities of β-Secretase to APP clusters, accounting for all possible outcomes. Furthermore we quantify how each of these scenarios may play out a role in pathological condition. For example, if APP clusters were to have much higher affinity to β-Secretase than APP monomers, we argue that under pathological over-expression of APP, there will be an increased number of clusters formed which will therefore result in excess Aβ formation. If the downstream reactions that produced Aβ were agnostic to whether APP was present in cluster form or monomer form, our model predicts the dynamics of how CTFβ formation would change for the different pathological conditions. With more experimental insights, based on the framework developed here our model parameters can be fine-tuned to address future questions that may arise. Therefore, newer constraints can be added to our model to predict with finer detail the role of APP and APP clustering in Aβ formation.

5 References

Alzheimer A. (1907). ber eine eigenartige Erkrankung der Hirnrinde. Allgemeine Zeitschrift fr Psychiatrie und Psychisch-Gerichtliche Medizine 64, 146148

Ben Halima S, Mishra S, Raja KMP, Willem M, Baici A, Simons K, Brstle O, Koch P, Haass C, Caflisch A and Rajendran L (2016). Specific Inhibition of β-Secretase Processing of the Alzheimer Disease Amyloid Precursor Protein. Cell Rep., 14 (2016), pp. 2127-2141

Cabrejo, L. et al. (2006). Phenotype associated with APP duplication in five families. Brain 129, 29662976

Claeysen, S. et al (2012). Alzheimer culprits: cellular crossroads and interplay. Cell Signal 24, 18311840

Glenner, G. G. and Wong, C. W. (1984). Alzheimer's disease: initial report of the purification and characterization of a novel cerebrovascular amyloid protein. Biochem. Biophys. Res. Commun. 120, 885890

Goedert, M., Wischik, C. M., Crowther, R. A., Walker, J. E. Klug, A. (1988). Cloning and sequencing of the cDNA encoding a core protein of the paired helical filament of Alzheimer disease: identification as the microtubule-associated protein τ. Proc. Natl Acad. Sci. USA 85, 40514055

Grundke-Iqbal, I. et al. (1986). Abnormal phosphorylation of the microtubule-associated protein τ (tau) in Alzheimer cytoskeletal pathology. Proc. Natl Acad. Sci. USA 83, 49134917

Gyure, K. A., Durham, R., Stewart, W. F., Smialek, J. E. Troncoso, J. C. (2001). Intraneuronal A-amyloid precedes development of amyloid plaques in Down syndrome. Arch. Pathol. Lab. Med. 125, 489492

Haass, C. et al. (1995). The Swedish mutation causes early-onset Alzheimer's disease by -secretase cleavage within the secretory pathway. Nature Med. 1, 12911296

Hill, A. V. (1910). "The possible effects of the aggregation of the molecules of hmoglobin on its dissociation curves". J. Physiol. 40 (Suppl): ivvii. doi:10.1113/jphysiol.1910.sp001386

Ihara, Y., Nukina, N., Miura, R. Ogawara, M. (1986). Phosphorylated τ protein is integrated into paired helical filaments in Alzheimer's disease. J. Biochem. (Tokyo) 99, 18071810

Kedia, S., Nair, D. and Ravindranath, V., $unpublished$

Koffie, R., Hyman, B. Spires-Jones, (2011). T. Alzheimer's disease: synapses gone

cold. Mol. Neurodegener. 6, 63

Kojro, E. and Fahrenholz, F. (2005). The non-amyloidogenic pathway: structure and function of -secretases. Subcell. Biochem. 38, 105127

Kosik, K. S., Joachim, C. L. Selkoe, D. J. (1986). Microtubule-associated protein tau (τ) is a major antigenic component of paired helical filaments in Alzheimer disease. Proc. Natl Acad. Sci. USA 83, 40444048
S. Kumari, M. G. Swetha and S. Mayor (2010). Endocytosis unplugged: multiple ways to enter the cell. Cell Res., 20, 256275
F.M. LaFerla, K.N. Green, S. Oddo. (2007). Intracellular amyloid- in Alzheimer's disease. Nat. Rev. Neurosci., 8 , pp. 499-509

Markesbery, W. R. (1997). Oxidative stress hypothesis in Alzheimer's disease. Free Radic. Biol. Med. 23, 134147

Masters, C. L. et al. (1985). Amyloid plaque core protein in Alzheimer disease and Down syndrome. Proc. Natl Acad. Sci. USA 82, 42454249

McGeer, P. L., Rogers, J. McGeer, E. G. (2006). Inflammation, anti-inflammatory agents and Alzheimer disease: the last 12 years. J. Alzheimers Dis. 9, 271276

Mori, C. et al. (2002). Intraneuronal A42 accumulation in Down syndrome brain. Amyloid 9, 88102

Rovelet-Lecrux, A. et al. (2006). APP locus duplication causes autosomal dominant early-onset Alzheimer disease with cerebral amyloid angiopathy. Nature Genet. 38, 2426

Rozemuller, J. M., Eikelenboom, P. Stam, F. C. (1986). Role of microglia in plaque formation in senile dementia of the Alzheimer type. An immunohistochemical study. Virchows Arch. B Cell Pathol. 51, 247254

Stiles, JR, and Bartol, TM. (2001). Monte Carlo methods for simulating realistic synaptic microphysiology using MCell. In: Computational Neuroscience: Realistic Modeling for Experimentalists, ed. De Schutter, E. CRC Press, Boca Raton, pp. 87-127

St George-Hyslop, P. H. and Petit, A. (2005). Molecular biology and genetics of Alzheimer's disease. C. R. Biol. 328, 119130

Westmeyer, G. G., Willem, M., Lichtenthaler, S. F., Lurman, G., Multhaup, G., Assfalg-Machleidt, I., et al. (2004). Dimerization of beta-site beta-amyloid precursor protein-cleaving enzyme. The Journal of Biological Chemistry, 279, 5320553212

Wyss-Coray, T. (2006). Inflammation in Alzheimer disease: driving force, bystander or beneficial response? Nature Med. 12, 10051015

6 Appendix on β-Secretase cleavage of APP in endocytic vesicles

The results in the appendix were incomplete at the time of the thesis submission deadline. They have been added as an appendix as advised by the TAC member.

6.1 Modelling APP activity in endocytic vesicles

As mentioned in the discussion, β-Secretase has increased activity for cleavage of APP inside endocytic vesicles, where there is an acidic pH($\sim$5.5). This ensures that at least the first step in processing of APP molecules happens inside these vesicles. These vesicles arise from the Peri-Synaptic membrane being pinched off to form spherical vesicles in a process called clathrin mediated endocytosis (S Kumari et al., 2010). These vesicles are usually large (120 - 150 nm in diameter) compared to synaptic vesicles and are formed only at the Peri-Synaptic region and not at other synaptic regions because Dynamin is highly localized to the Peri-Synaptic region and is known to be necessary to kick start clathrin-mediated endocytosis.

To model the phenomenon of β-Secretase cleavage of APP in endocytic vesicles, we first create a spherical vesicle of diameter 120 nanometers (as shown in Figure 17). As we are interested in studying the role of APP clusters in relation to the formation of CTFβ, we simulate a scenario with an APP cluster on the vesicle and a scenario without an APP cluster on the vesicle. For the size and density of the cluster, we pick a cluster with area 0.006 μm^2 containing 20 APP molecules (taken from Kedia et al., unpublished). For the vesicle containing the APP cluster, we release 25 APP monomers and one cluster containing 20 APP molecules. For the vesicle without the APP cluster, we release 45 monomers. Approximately 250 β-Secretase molecules are released uniformly on both the vesicles. The diffusion coefficient of the APP molecules in the cluster is taken to be 1×10^{-2} $\mu m^2/sec$ and those of APP in monomer form is taken to be 7×10^{-2} $\mu m^2/sec$. Since β-Secretase is a single pass trans-membrane protein(just like the APP monomer) and its diffusion coefficient has been estimated to be of the same order of magnitude as the APP monomer, we assume that the diffusion coefficient for β-Secretase monomer is 7×10^{-2} $\mu m^2/sec$ and the β-Secretase present in cluster is 1×10^{-2} $\mu m^2/sec$.

To simulate the reaction, we assume the secretase cleavage follows Michaelis-Menten kinetics. Michaelis-Menten kinetics has been assumed for this reaction previously in literature as well(HS Ben et al., 2016). From this reference, we obtained the k_{cat}(catalytic rate) and the k_M(the Michaelis constant). The catalytic rate is independent of concentration and depends only inversely on time. The Michaelis constant is proportional to concentration(HS Ben et al., 2016). As these constants were obtained experimentally under conditions that facilitated 3-D diffusion of molecules, only the k_{Cat} value was taken exactly from their data(as it does not depend on concentration) while the k_1 and k_{-1} were left as open parameters.

To simulate the processing of APP-Swedish by β-Secretase, we used k_{Cat} values provided by HS Ben et al., 2016. Since the K_M value was approximately 7 times lesser,

we reduced the value in our simulation by the same scaling factor. The diffusion coefficients for APP-Swedish monomers and APP-Swedish present as clusters were provided by Kedia et al., unpublished.

6.2 Difference in processing of APP monomers and APP clusters by β-Secretase

As shown in Figure 14, we simulate two vesicles for a duration of 1 second, one with an APP cluster and one without. For the reaction rates, we set the K_{Cat} value as 2×10^{-3} s^{-1} for APP Wild-Type cleavage by β-Secretase and 2.5×10^{-2} s^{-1} for APP Swedish cleavage by β-Secretase. We keep the k_1 and the k_{-1} values as open parameters. We constrain the values of k_1 and the k_{-1} by ensuring that there are a few intermediates present at all times and not all the APP is processed by β-Secretase.
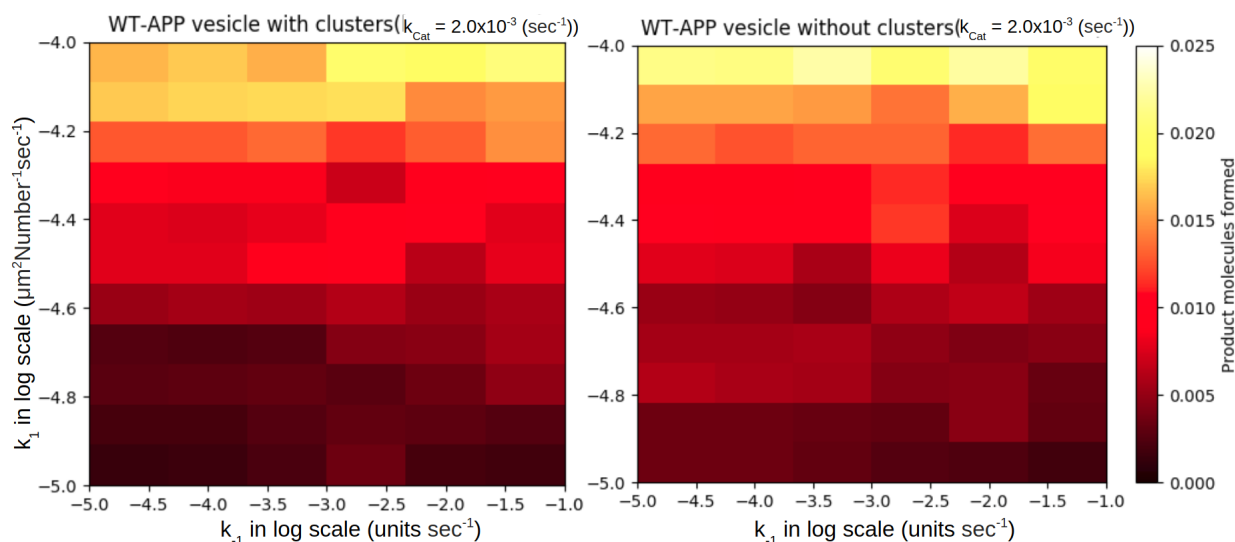

Figure 19: Number of CTFβ molecules produced in vesicles with WT-APP, with and and without APP clusters. The open parameters in this plot are the forward and backward rates k_1 and k_{-1} which are plotted on the Y and X-axis respectively. The Z-axis or the colour represents the number of product molecules(CTFβ) formed. The plot on the left shows the number of product molecules formed in the vesicle with the APP cluster and the plot on the right represents the number of product molecules formed in the vesicle without the cluster. This simulation has been run for a total of 5000 iterations for each set of rates to determine the average behaviour for the given rates.

We then compare the differences in the number of product molecules formed for the vesicles with and without clusters for a given set of rates. Each unique set of rates is run for 5000 different random initiations(seeds) and the average behaviour is plotted in Figure Y. As highlighted in Figure Y, we see many sets of reaction rates that have a significantly higher production of CTFβ in the vesicles without an APP cluster when compared to vesicles with APP clusters. We used the Mann-Whitney U test to quantify the difference between the two cases(as shown in Figure P).
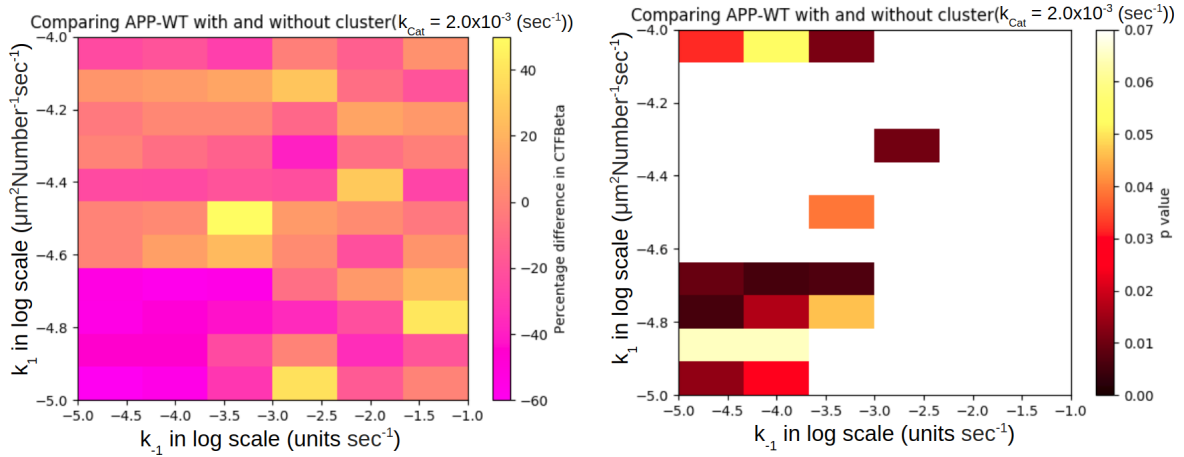
Figure 20: Percentage difference in CTFβ molecules produced in vesicles with WT-APP, with and and without APP clusters. The open parameters in this plot are the forward and backward rates k_1 and k_{-1} which are plotted on the Y and X-axis respectively. The Z-axis or the colour for the plot on the left represents the percentage change in number of CTFβ molecules formed in vesicles with clusters when compared to vesicles without clusters. The Z-axis or the colour for the plot on the right represents the p-value quantifying the significance in the difference between the behaviour of vesicles with and without clusters. This simulation has been run for a total of 5000 iterations for each set of rates to determine the average behaviour for the given rates. The conclusion from this figure is that all the statistically significant differences in product formed correspond to a decrease in CTFβ in vesicles containing clusters.

From this we can conclude for certain reaction rates, APP clusters are more protected from forming CTFβ molecules when compared to APP monomers.

6.3 Difference in processing of APP wild-type and APP-Swedish by β-Secretase

To simulate the amount of production of CTFβ under APP-Swedish conditions, we use the diffusion and rate values as listed in Section 6.1. Again, we do the simulations with a vesicle containing a single APP cluster and a vesicle containing no APP clusters.

To quantify the differences in CTFβ production in the vesicles with and without a cluster, we use the Mann-Whitney U test. We see a similar result as in the wild-type APP where there are some sets of rates that have a higher production of CTFβ in the vesicles without clusters when compared to the vesicles with clusters.

In comparison to the wild-type, the vesicles with APP-Swedish produce much more CTFβ for the same density of APP and β-Secretase molecules. This concurs with the fact that APP-Swedish has a much higher risk of resulting in AD when compared to wild-type APP.
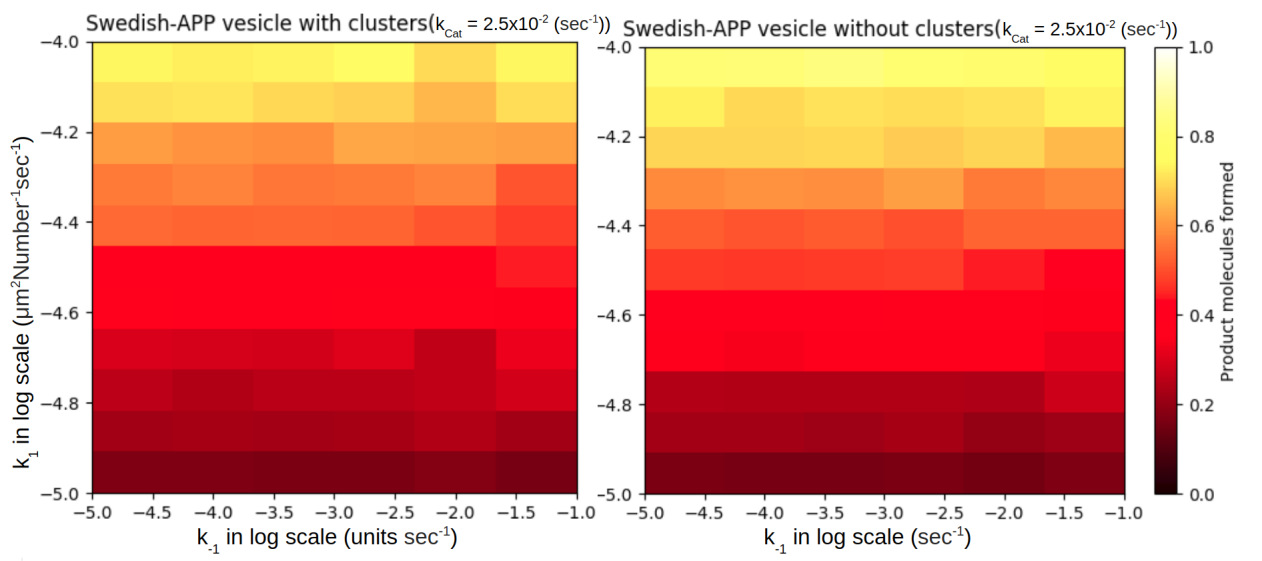
Figure 21: Number of CTFβ molecules produced in vesicles with APP-Swedish, with and and without APP clusters. The open parameters in this plot are the forward and backward rates k_1 and k_{-1} which are plotted on the Y and X-axis respectively. The Z-axis or the colour represents the number of product molecules(CTFβ) formed. The plot on the left shows the number of product molecules formed in the vesicle with the APP cluster and the plot on the right represents the number of product molecules formed in the vesicle without the cluster. This simulation has been run for a total of 1000 iterations for each set of rates to determine the average behaviour for the given rates.
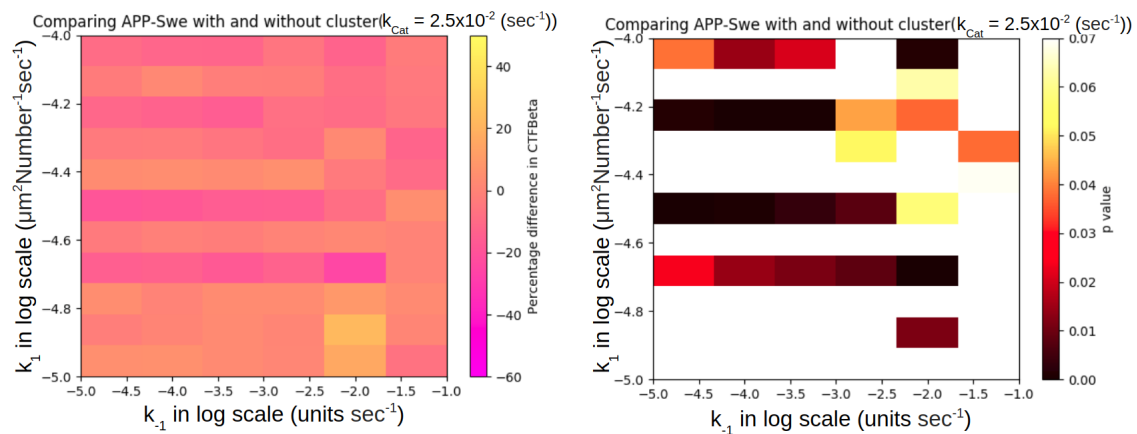
Figure 22: Percentage difference in CTFβ molecules produced in vesicles with APP-Swedish, with and and without APP clusters. The open parameters in this plot are the forward and backward rates k_1 and k_{-1} which are plotted on the Y and X-axis respectively. The Z-axis or the colour for the plot on the left represents the percentage change in number of CTFβ molecules formed in vesicles with clusters when compared to vesicles without clusters. The Z-axis or the colour for the plot on the right represents the p-value quantifying the significance in the difference between the behaviour of vesicles with and without clusters. This simulation has been run for a total of 1000 iterations for each set of rates to determine the average behaviour for the given rates. The conclusion from this figure is that all the statistically significant differences in product formed correspond to a decrease in CTFβ in vesicles containing clusters, similar to the conclusion in the vesicles containing APP-WT.